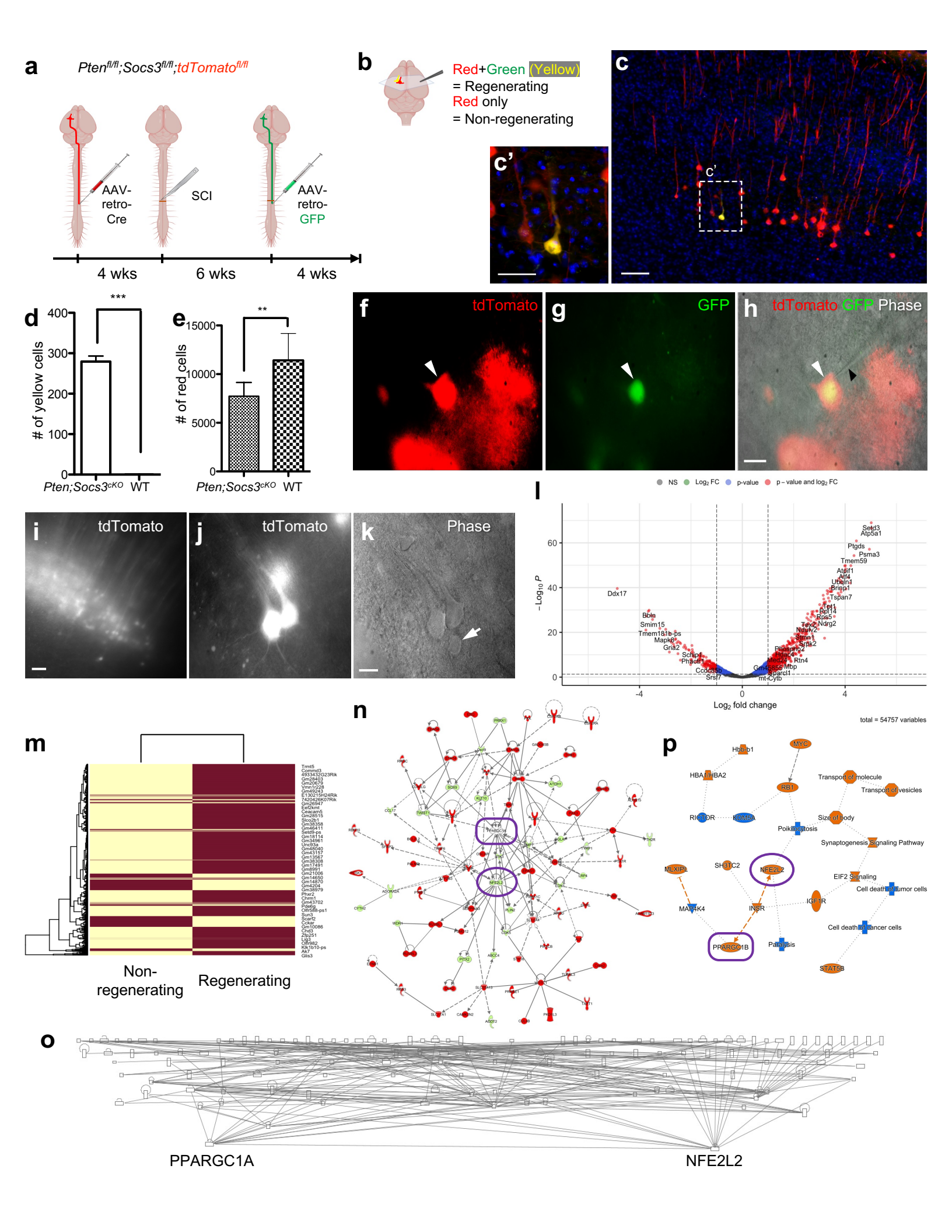
a
Pten^fl/fl;Socs3^fl/fl;tdTomato^fl/fl
AAV-retro-Cre
SCI
AAV-retro-GFP
4 wks
6 wks
4 wks
b
Red+Green (Yellow) = Regenerating
Red only = Non-regenerating
c
c'
d
# of yellow cells
***
Pten;Socs3cKO
WT
e
# of red cells
**
Pten;Socs3cKO
WT
f tdTomato
g GFP
h tdTomato GFP Phase
i tdTomato
j tdTomato
k Phase
l
NS
Log2 FC
p-value
p – value and log2 FC
−Log10 P
Log2 fold change
m
Non-regenerating
Regenerating
n
total = 54757 variables
p
o
PPARGC1A
NFE2L2

**Fig. 1. Patch-based scRNA-Seq analyses of regenerating CST neurons identify *NFE2L2* and *PPARGC1A* as two central hubs in gene network. a**, Surgical timeline. SCI, dorsal hemisection spinal cord injury. With dual retrograde AAV tracing with one virus before and another after injury, regenerating CST neurons would be labeled in both green and red (yellow) while non-regenerating neurons will be labeled in red only (b). **c**, Representative immunohistochemical image of retrograde AAV traced CST neurons in cortical layer 5 illustrating the low incidence of regeneration by CST neurons (red + green = yellow) following *PTEN* and *SOCS3* deletion. Scale Bar = 100 μm; 20 μm (c' high mag). **d**, Quantification on regenerating CST neurons (red + green) following *PTEN* and *SOCS3* deletion per mouse. N = 2 (WT); 2 (double mutant). **e**, Quantification of total numbers of retrogradely labeled CST neurons (red, including both regenerating and non-regenerating). ***$p < 0.001$, **$p < 0.01$, two-tailed unpaired t test. **f**-**h**, Patch clamp collection of a regenerating CST neuron marked by both tdTomato and GFP (white arrowhead) from an acute brain slice. In (h), tdTomato, GFP channels are merged with phase contrast taken from a patch rig at high magnification, where black arrowhead marks the patch pipette approaching the doubly labeled neuron. **i**, Many tdTomato fluorescent CST neurons in the area of interest can be seen at low magnification in the brain slice. **j**,**k**, tdTomato positive neurons neighboring a tdTomato negative cell (white arrow). Scale Bar = 100 μm (i), 20 μm (f-h, j, k). **l**, Volcano plot of differentially expressed (DE) genes. Large number of genes were significantly (adjusted p-value<0.05) overexpressed in regenerating neurons. **m**, Heatmap of DE gene expression of regenerating and non-regenerating neurons (yellow: low; brown: high in regenerating neurons). **n**, Gene network analysis with IPA using main genes with overexpressed and underexpressed genes indicates that NFE2L2 and PPARGC1A are represented as central regulators of these genes. Red: overexpressed genes; Green: underexpressed genes. **o**, Full network analysis illustrates NFE2L2 and PPARGC1A as two top regulators of DE genes. **p**, Graphical summary of core analysis also implicates NFE2L2 in the center of the network. Note that PPARGC1B (instead of PPARGC1A) is a node in this network.

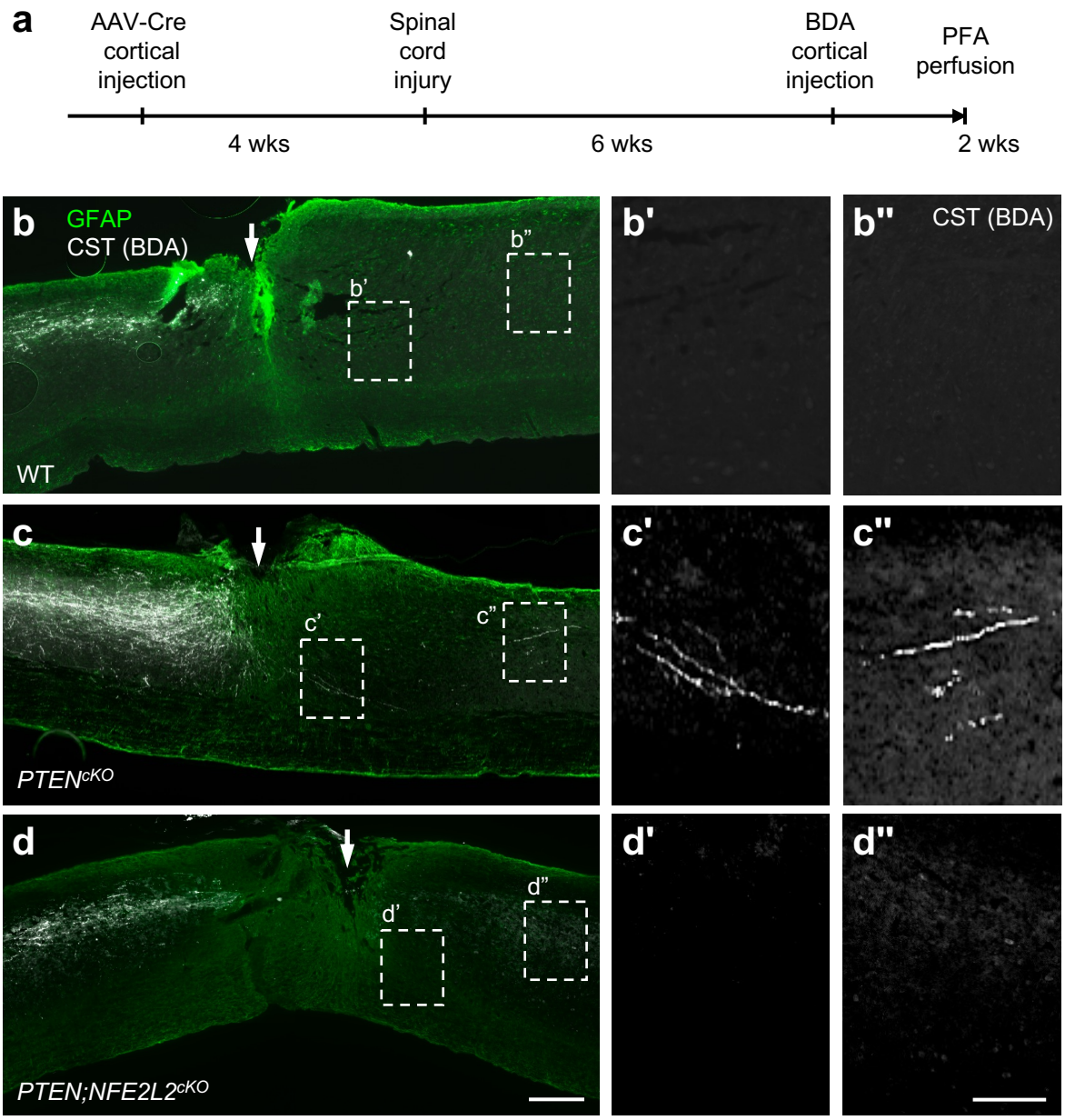
a
AAV-Cre cortical injection
Spinal cord injury
BDA cortical injection
PFA perfusion
4 wks
6 wks
2 wks
b
GFAP
CST (BDA)
b'
b''
WT
c
c'
c''
PTEN^cKO
d
d'
d''
PTEN;NFE2L2^cKO
e
Axon density index
Rostral distance from injury
f
Axon number index
Caudal distance from injury
PTEN;NFE2L2^cKO
PTEN^cKO
WT

**Fig. 2. *NFE2L2* gene deletion substantially diminishes *PTEN* deletion-induced CST axon regeneration. a**, Experimental timeline. **b**-**d**, Representative sagittal thoracic spinal cord sections showing BDA-traced CST axons at and around the T8 dorsal hemisection spinal cord injury site (arrow) from wild-type (WT), *PTEN* conditional knockout (cKO), and *PTEN;NFE2L2* double conditional knockout mice. Rostral is to the left; caudal is to the right. Selected areas in dotted boxes in low magnification images on the left are shown at high magnification on the right. Scale bar = 300 μm (b-d, low mag), 100 μm (b'-d", high mag). **e**, Quantification of axon density indices rostral to injury. Axon density indices were calculated as the average axon intensity at defined distances rostral to injury, and then normalized to axon density at 1.4-1.5 mm rostral to injury (mean ± SEM). Two-way RM ANOVA revealed significant differences across genetic conditions. Multiple comparisons with Bonferroni correction revealed elevated densities in $PTEN^{cKO}$ multiple distance from injury site. *p < 0.05 at 700 μm ; **p < 0.01 at 600-300 μm;, ***p < 0.001 at 200 μm. PTEN;NFE2L2$^{cKO}$ showed significantly elevated densities at 500 μm, **p < 0.01; at 400 μm and 200 μm, *p < 0.05. **f**, Quantification of axon number indices caudal to the injury site. Axon number indices were calculated as the average axon numbers at defined distances caudal to injury and then normalized to total axon count labeled in the medulla. Two-way RM ANOVA revealed statistically significant differences across genetic conditions. Multiple comparisons with Bonferroni correction revealed significantly elevated regeneration for $PTEN^{cKO}$: ***p < 0.001 at 50–150 μm, **p < 0.01 ; at 200 μm. Annotations for statistics for 2c and 2d: *p < 0.05, **p < 0.01, ***p < 0.001. N = 7 (WT), 10 ($PTEN^{cKO}$), 7 ($PTEN;NFE2L2^{cKO}$).

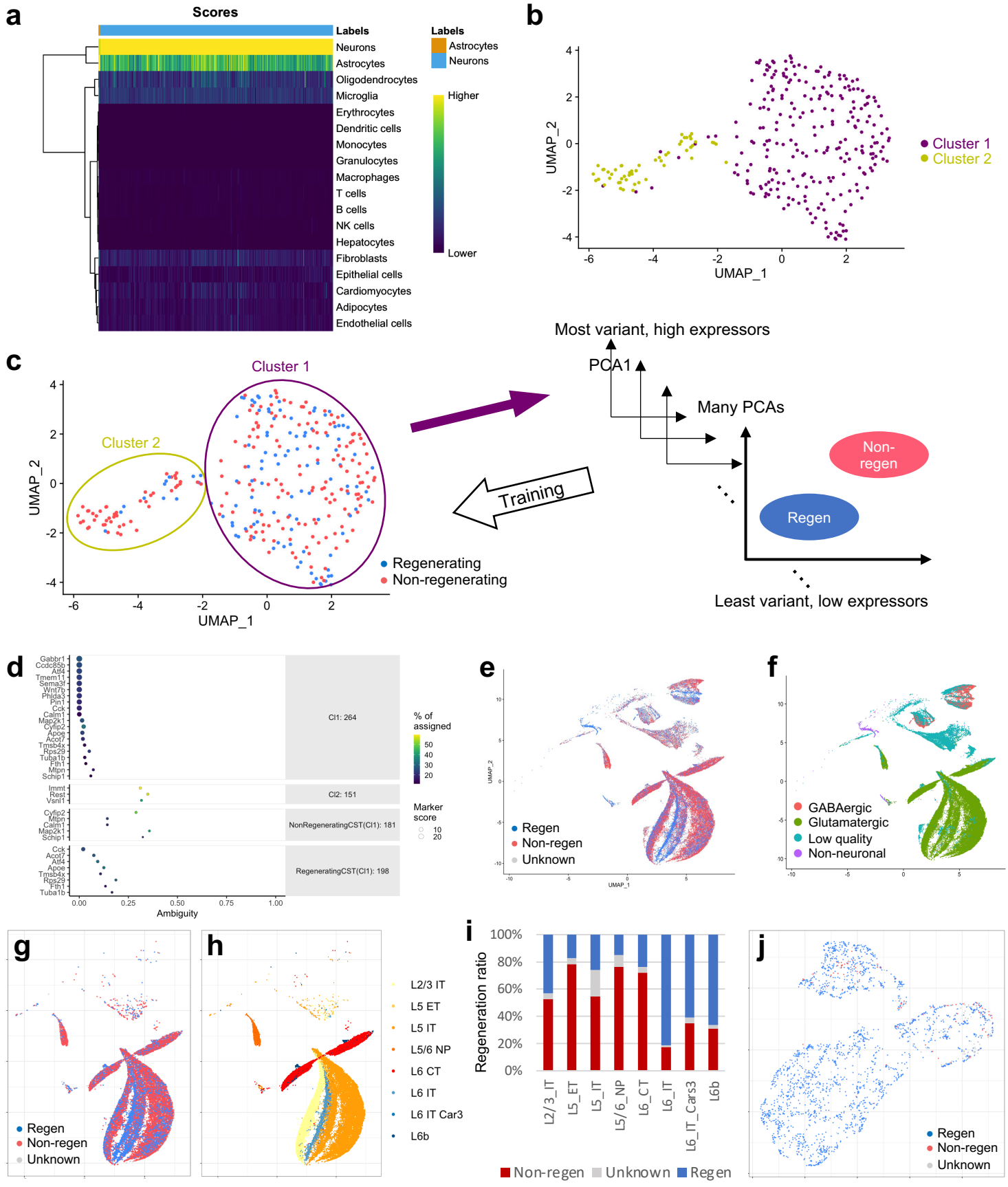
a
Scores
Labels
Neurons
Astrocytes
Oligodendrocytes
Microglia
Erythrocytes
Dendritic cells
Monocytes
Granulocytes
Macrophages
T cells
B cells
NK cells
Hepatocytes
Fibroblasts
Epithelial cells
Cardiomyocytes
Adipocytes
Endothelial cells
Labels
Astrocytes
Neurons
Higher
Lower
b
UMAP_2
UMAP_1
Cluster 1
Cluster 2
c
Cluster 1
Cluster 2
UMAP_2
UMAP_1
Regenerating
Non-regenerating
Training
Most variant, high expressors
PCA1
Many PCAs
Non-regen
Regen
Least variant, low expressors
d
Gabbr1
Ccdc85b
Atf4
Tmem11
Sema3f
Wnt7b
Phlda3
Pin1
Cck
Calm1
Map2k1
Cyfip2
Apoe
Acot7
Tmsb4x
Rps29
Tuba1b
Fth1
Mtpn
Schip1
Immt
Rest
Vsnl1
Cyfip2
Mtpn
Calm1
Map2k1
Schip1
Cck
Acot7
Atf4
Apoe
Tmsb4x
Rps29
Fth1
Tuba1b
Cl1: 264
Cl2: 151
NonRegeneratingCST(Cl1): 181
RegeneratingCST(Cl1): 198
0.00
0.25
0.50
0.75
1.00
Ambiguity
% of assigned
50
40
30
20
Marker score
10
20
e
Regen
Non-regen
Unknown
f
GABAergic
Glutamatergic
Low quality
Non-neuronal
g
Regen
Non-regen
Unknown
h
L2/3 IT
L5 ET
L5 IT
L5/6 NP
L6 CT
L6 IT
L6 IT Car3
L6b
i
Regeneration ratio
100%
80%
60%
40%
20%
0%
L2/3_IT
L5_ET
L5_IT
L5/6_NP
L6_CT
L6_IT
L6_IT_Cars3
L6b
Non-regen
Unknown
Regen
j
Regen
Non-regen
Unknown

**Fig. 3. Single cell clustering analysis on Patch-Seq'ed corticospinal neurons. a**, Cell type analysis using SingleR. The most expressed markers were neuronal markers. The vast majority of cells were classified as neurons. **b**, UMAP representation of unsupervised single cell clustering by Seurat.. **c**, Developing Regeneration Classifier (RC) with machine learning of single cell data with Garnett. **d**, Main Markers used as initial categorization of Regeneration Classifier and ambiguity testing of regenerating/non-regenerating markers on all clusters (Cluster 1,2 and Regen/Non-regen). **e**-**i**, Applying RC to a published dataset on neurons from the mouse primary motor cortex (Yao et al., 2021) illustrate regenerative heterogeneity. **e**, UMAP plot after applying RC to all cells; **f**, Original UMAP plot of all cells; **g**, UMAP plot after applying RC to glutamatergic neurons only; **h**, Original UMAP showing sub-classification of glutamatergic neurons based on cortical layers and axonal projections; **i**, Regeneration ratio plot (including regenerating, non-regenerating and unknown) for different subtypes of glutamatergic neurons after applying the RC. **j**, Applying RC to neurons from raphe nuclei (Okaty et al., 2020). Note most neurons from raphe nuclei are classified as regenerators.

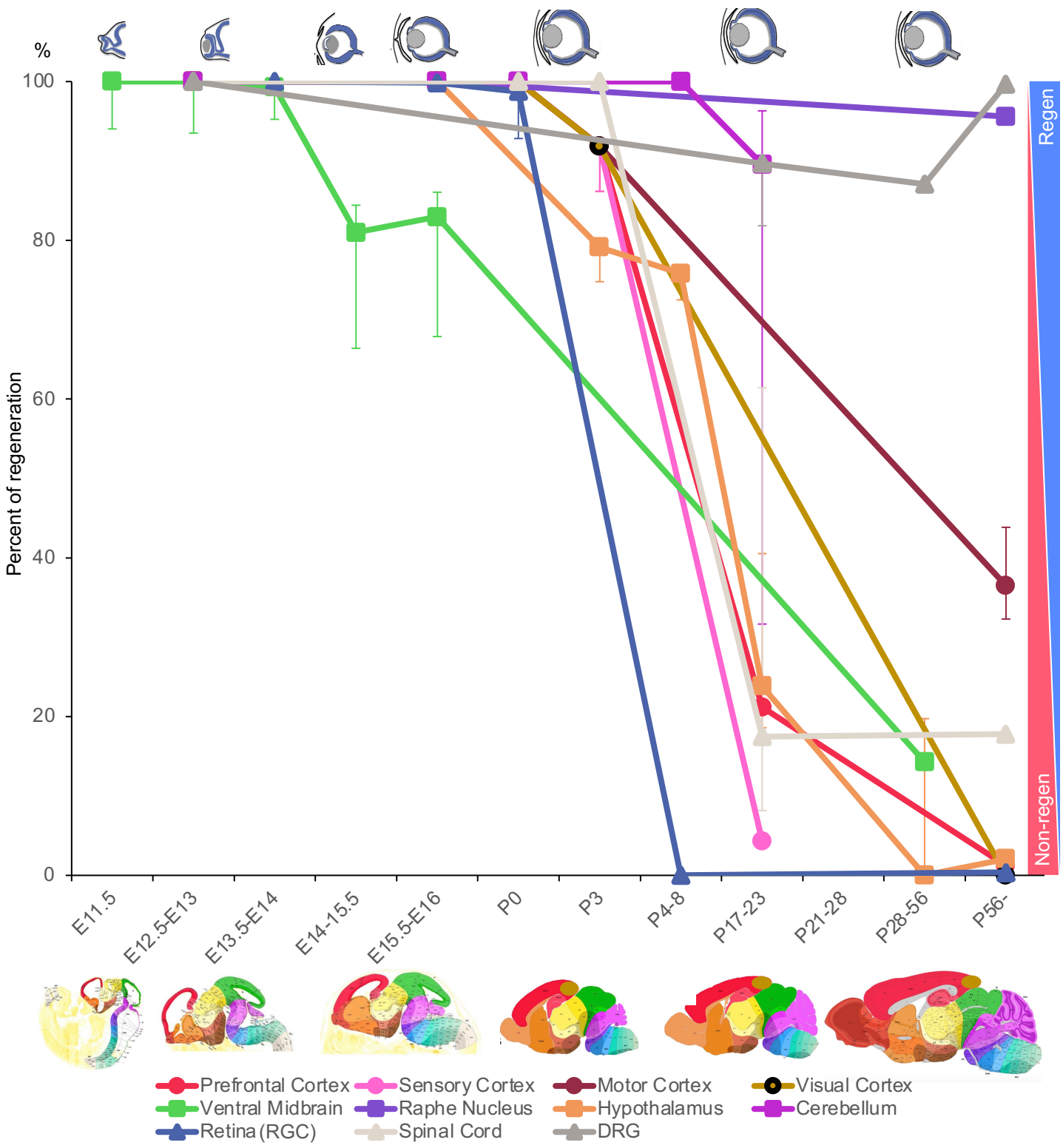
%
100
80
60
40
20
0
Percent of regeneration
Regen
Non-regen
E11.5
E12.5-E13
E13.5-E14
E14-15.5
E15.5-E16
P0
P3
P4-8
P17-23
P21-28
P28-56
P56-
Prefrontal Cortex
Sensory Cortex
Motor Cortex
Visual Cortex
Ventral Midbrain
Raphe Nucleus
Hypothalamus
Cerebellum
Retina (RGC)
Spinal Cord
DRG

**Fig. 4. Applying Regeneration Classifier to published scRNA-Seq data generates cell type- and developmental stage-appropriate classifications.** There is a general trend for development dependent decline in regeneration potential, with some neuronal populations being more resistant to this decline such as neurons in DRGs (dorsal root ganglia) and the raphe nuclei. Regeneration ratio is calculated as the number of regenerating neurons over the sum of regenerating and non-regenerating neurons, with the assumption that unknowns are in the same ratio as regenerating and non regenerating neurons for the first approximation. Error bars mark the extreme cases where all the unknowns are non-regenerating at the low end or regenerating at the high end. For prefrontal, sensory, motor and visual cortices, the earlier data points were from the forebrain; for raphe nucleus, hypothalamus and cerebellum, the earlier data points were from the hindbrain.

ScRNA-Seq data source:
Prefrontal cortex: Jessa et al., 2019 (E12.5-P3/Forebrain), Bhattacherjee et al 2019 (P21, P28-56)
Sensory cortex: Jessa et al., 2019 (E12.5-P3/Forebrain), Zeisel et al. 2015 (P21)
Motor cortex: Jessa et al., 2019 (E12.5-P3/Forebrain), Yao et al. 2022 (P56)
Visual cortex: Jessa et al., 2019 (E12.5-P3/Forebrain), Tasic et al. 2015 (P56)
Ventral midbrain: La Manno et al., 2016 (E11.5-E18.5, P28-56)
Raphe nucleus: Jessa et al., 2019 (E12.5-E16/Hindbrain), Okaty et al. 2020 (P35-70)
Hypothalamus: Jessa et al., 2019 (E12.5-P6 /Hindbrain), Romanov et al. 2017 (Juvenile), Campbell et al., 2017 (Adult), Chen et al., 2017 (P56)
Cerebellum: Jessa et al. 2019 E12.5-E16/Hindbrain), Peng et al., 2019 (P0,P8), Zeisel et al., 2018 (P20)
Retina (RGCs): Shekhar et al. 2022 (E13-P5), Tran et al., 2019 (P56)
Spinal cord: Delile et al., 2019 (E9.5-13.5), Liau et al., 2023 (E13.5), Hayshi et al., 2018 (P0-3), Zeisel et al., 2018 (P20), Hairing et al., 2018 (P21-28), Milich et al., 2020 (Adult)
DRG: Zeisel et al., 2018 (P20), Zeisel et al., 2018 (P20), Usoskin et al., 2015 (P42-56), Avraham et al., 2020 (P56-)

Note that DRGs exhibit a dip and then recovers likely due to the small sample size and/or the use of older technologies Zeisel et al., 2018 and Usoskin et al., 2015.

Retina diagrams: modified from Beby and Lamonerie, 2013
Brain diagrams: modified from Thompson et al., 2014.

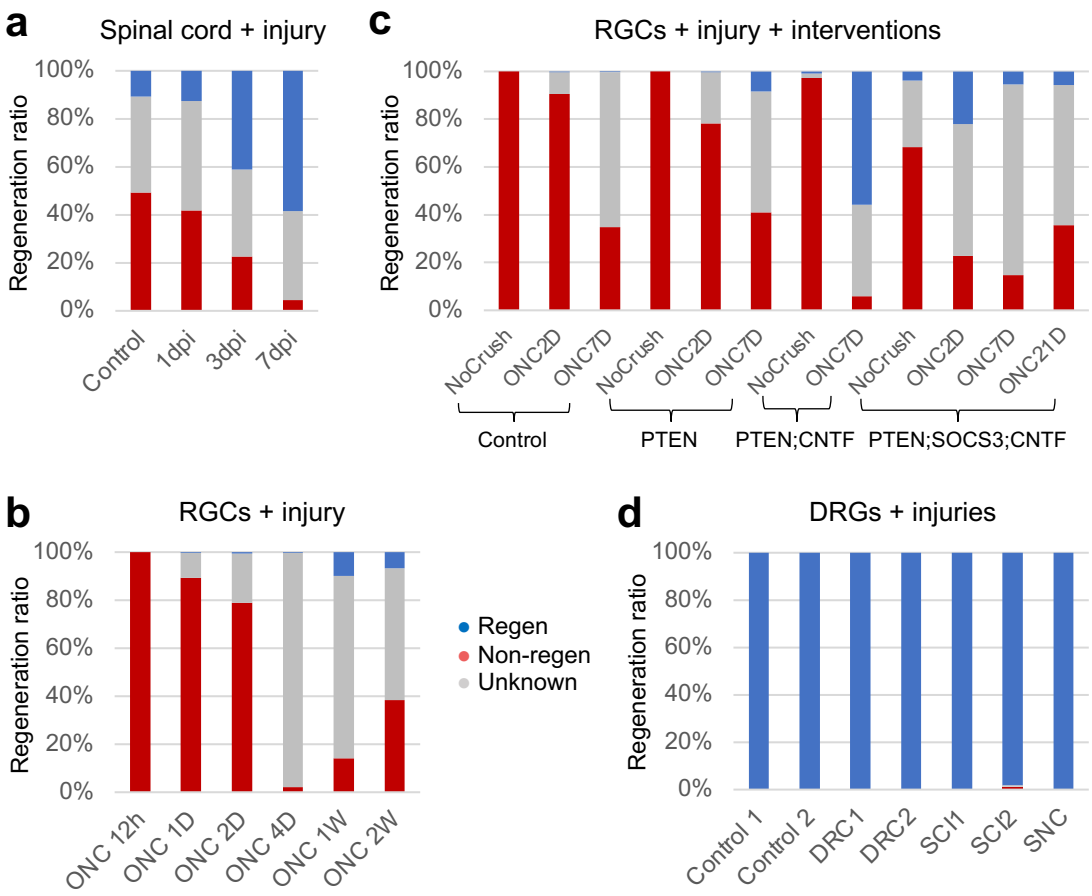


**Fig. 5. Applying Regeneration Classifier to neurons after injury reveals neuron type-specific responses. a-d**, Regeneration ratio plots on scRNA-Seq data from spinal neurons around a spinal cord injury site (a), retinal ganglion cells (RGCs) after optic nerve crush without molecular interventions (b), RGCs after optic nerve crush with molecular interventions (PTEN/SOCS3 conditional knockout, and/or CNTF overexpression), dorsal root ganglion (DRG) neurons after various injuries. Note that the control RGC profile especially at 7 days after optic nerve crush in (c) appears different from that in (b), likely reflecting some inter-study variability even within the same research team. SNC, sciatic nerve crush; DRC, dorsal root crush; SCI, spinal cord injury. ScRNA-Seq data source: Milich et al. 2021 (a); Tran et al., 2019 (b); Jacobi et al., 2022 (c); Avraham et al. 2021 (d). *The corresponding UMAP plots for panels (a-d) are shown in Extended Data Figs. 7-10 respectively.*

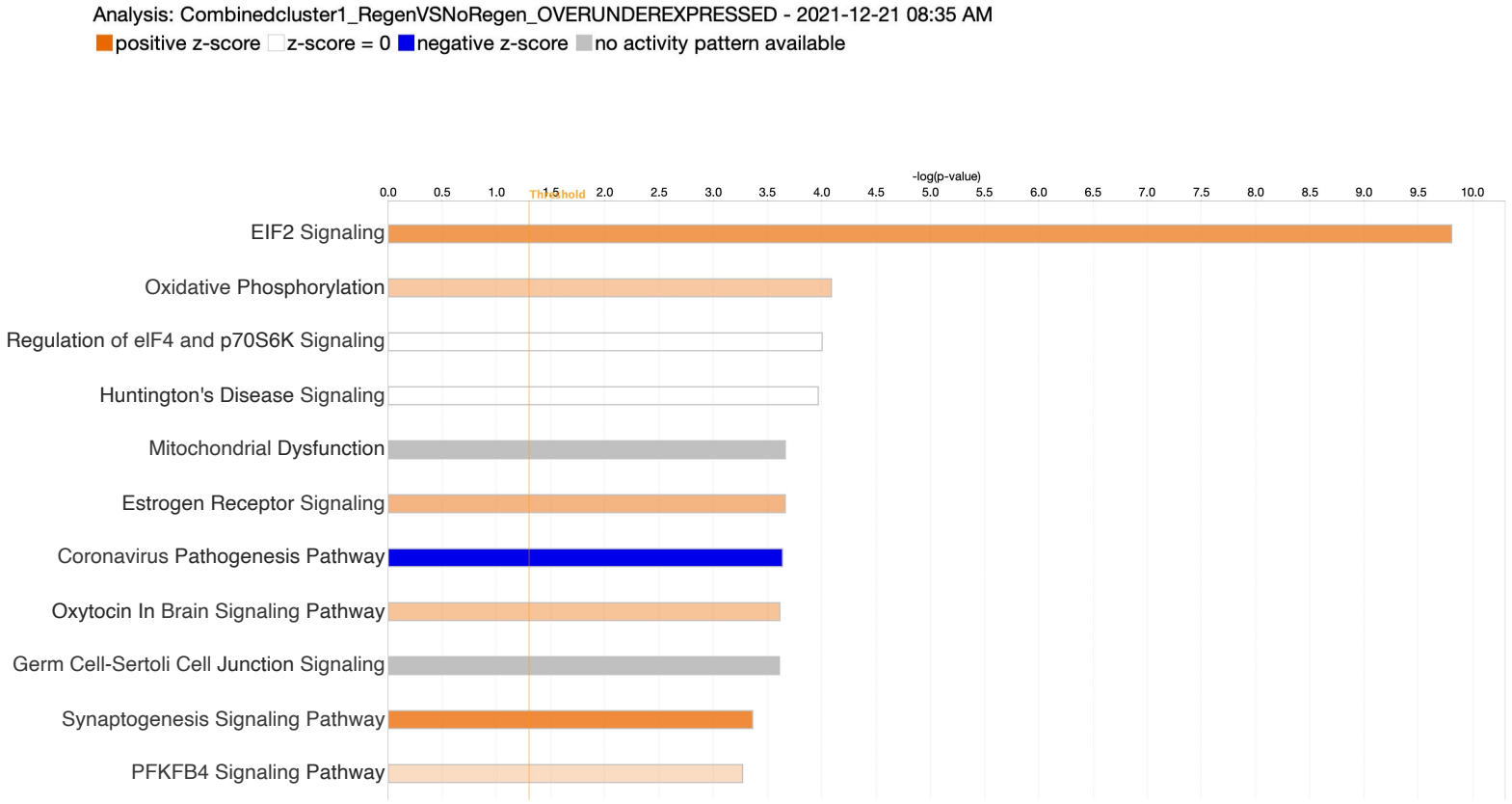


**Extended Data Fig. 1. Top canonical pathways identified from differentially expressed genes between regenerating and non-regenerating CST neurons.** The EIF2 Signaling pathway is the most significantly activated pathway followed by Oxidative Phosphorylation.

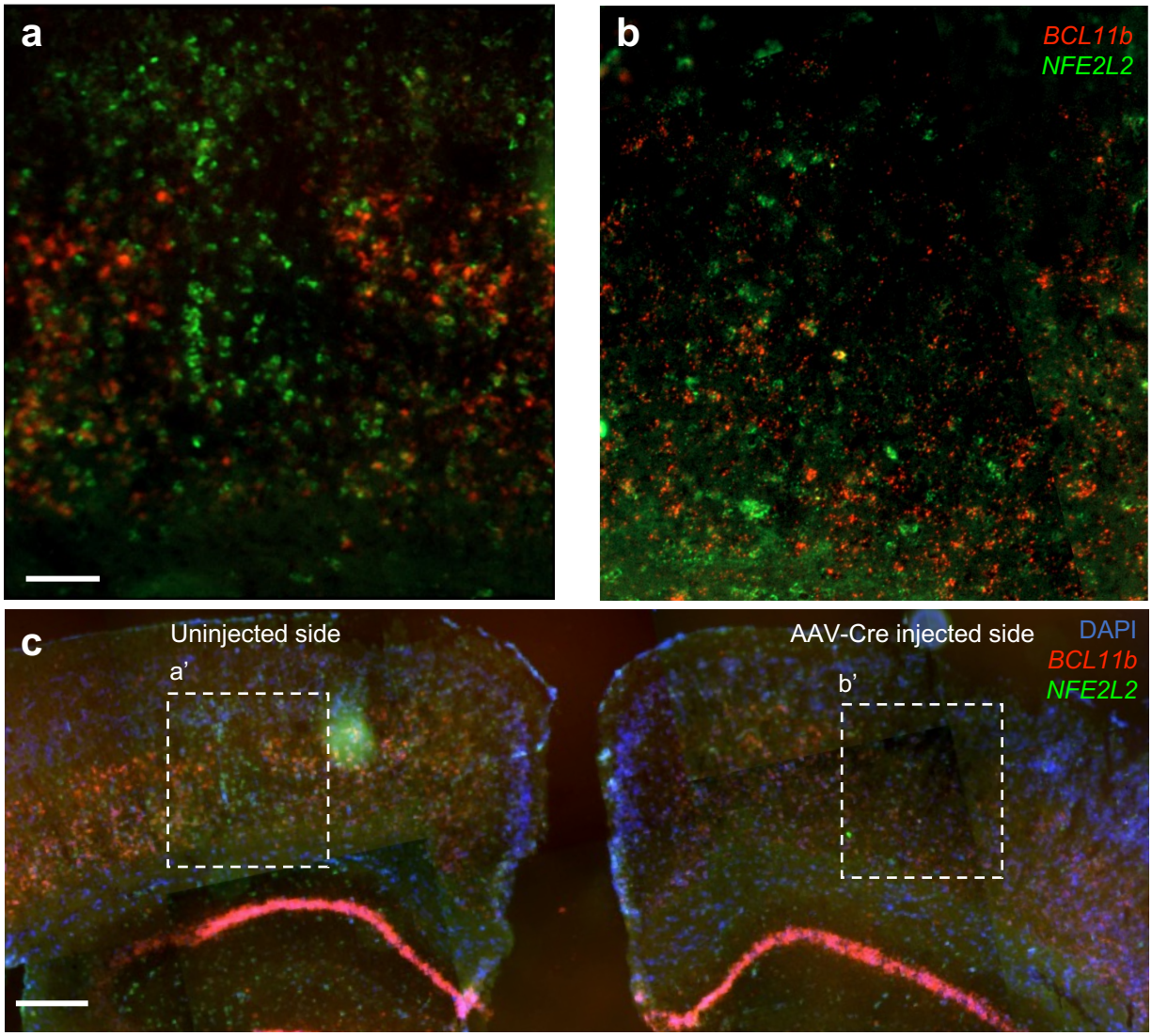


**Extended Data Fig. 2. RNAScope validation of conditional *NFE2L2* gene deletion. a**,**b**, High magnification images showing *NFE2L2* (green) and *BCL11b* (red) mRNA expression by RNAScope on the uninjected side (a) and the AAV-Cre injected side (b). **c**, Low magnification image (taken with 5x objective) showing the entire region with DAPI nuclear counterstain. Scale bar = 100 μm (a, b), 500 μm (c). *BCL11b* is also known as *CTIP2*, commonly used as a marker for CST neurons.

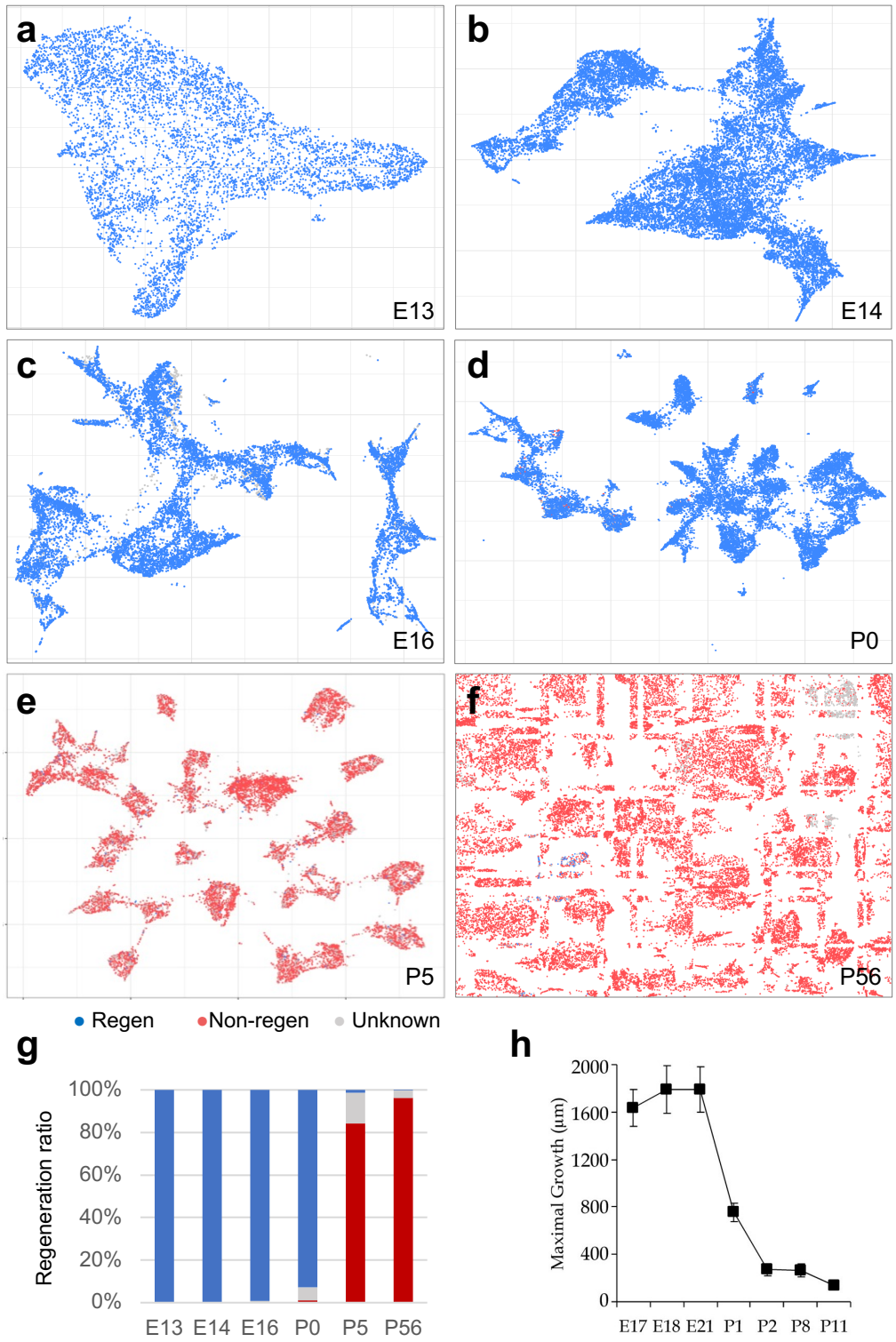


**Extended Data Fig. 3. Applying Regeneration Classifier to retinal ganglion cells (RGCs) and across developmental stages. a-f**, UMAP plots of scRNA-Seq data on RGCs from different developmental stages, color coded for regeneration classifications. All panels show RGCs only unless marked with circles, which encircle neurons among all cell types sequenced. **g**, Regeneration ratio plot based on the regeneration classifications. Sc-RNA Seq data source: E13 – P5, Shekhar et al. 2022; P56, Tran et al., 2019 (both papers were published by the same research team). **h**, Intrinsic axon growth ability of in vitro cultured RGCs isolated from rats of different ages reported by Goldberg et al., 2002. Note the striking resemblance on the developmental decline in (g) and (h).

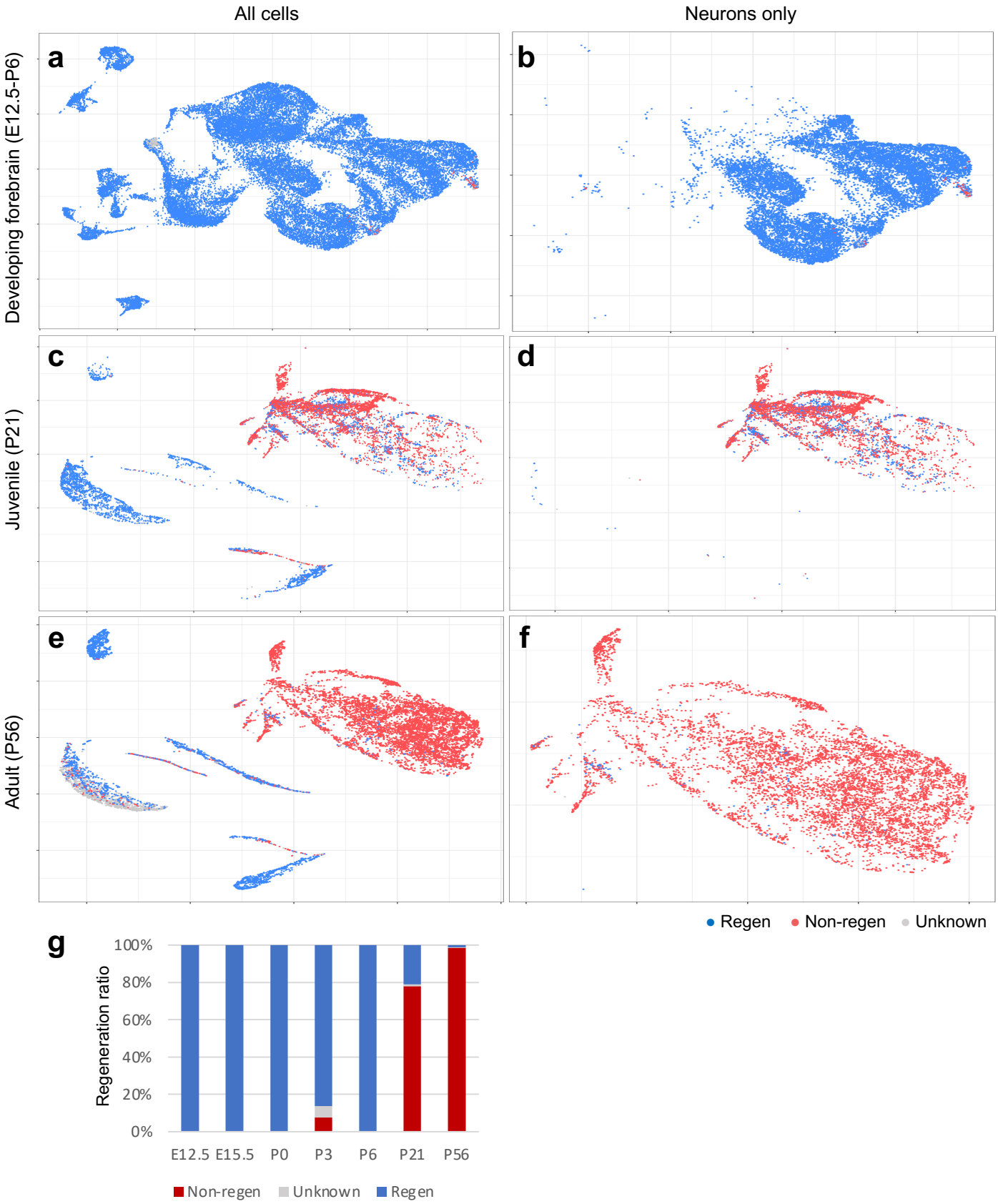


**Extended Data Fig. 4. Applying Regeneration Classifier to the prefrontal cortex across developmental stages. a-f**, UMAP plots of scRNA-Seq data on all cells (a, c, e) or neurons only (b, d, f) from the prefrontal cortex at different developmental stages, color coded for regeneration classifications. Note that data from E12.5 to P6 were from forebrain and not prefrontal cortex specifically, when most neurons were classified as regenerators (P6 dataset included only a very small number of cells). **g**, Regeneration ratio plot on neurons only. ScRNA-Seq data source: E12.5-P3, Jessa et al., 2019; P21-P56, Bhattacherjee et al., 2019.

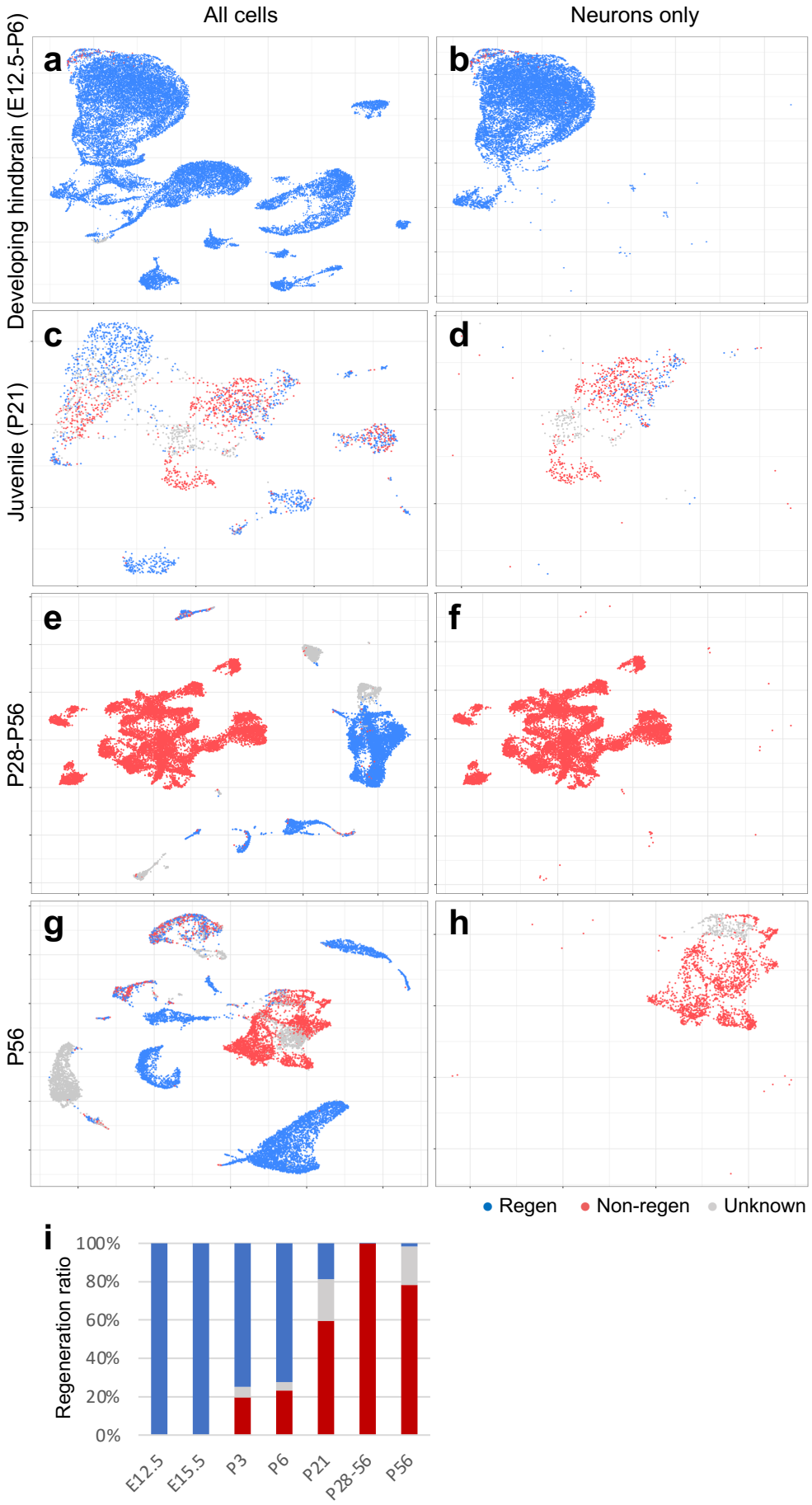


**Extended Data Fig. 5. Applying Regeneration Classifier to the hypothalamus across developmental stages.** **a-h**, UMAP plots of scRNA-Seq data on all cells (a, c, e, g) or neurons only (b, d, f, h) from the hypothalamus at different developmental stages, color coded for regeneration classifications. **i**, Regeneration ratio plot. ScRNA-Seq data source: E12.5-P3, Jessa et al., 2019 (hind brain); P21, Romanov et al., 2019; P28-56, Campbell et al., 2017, P56, Chen et al., 2017.

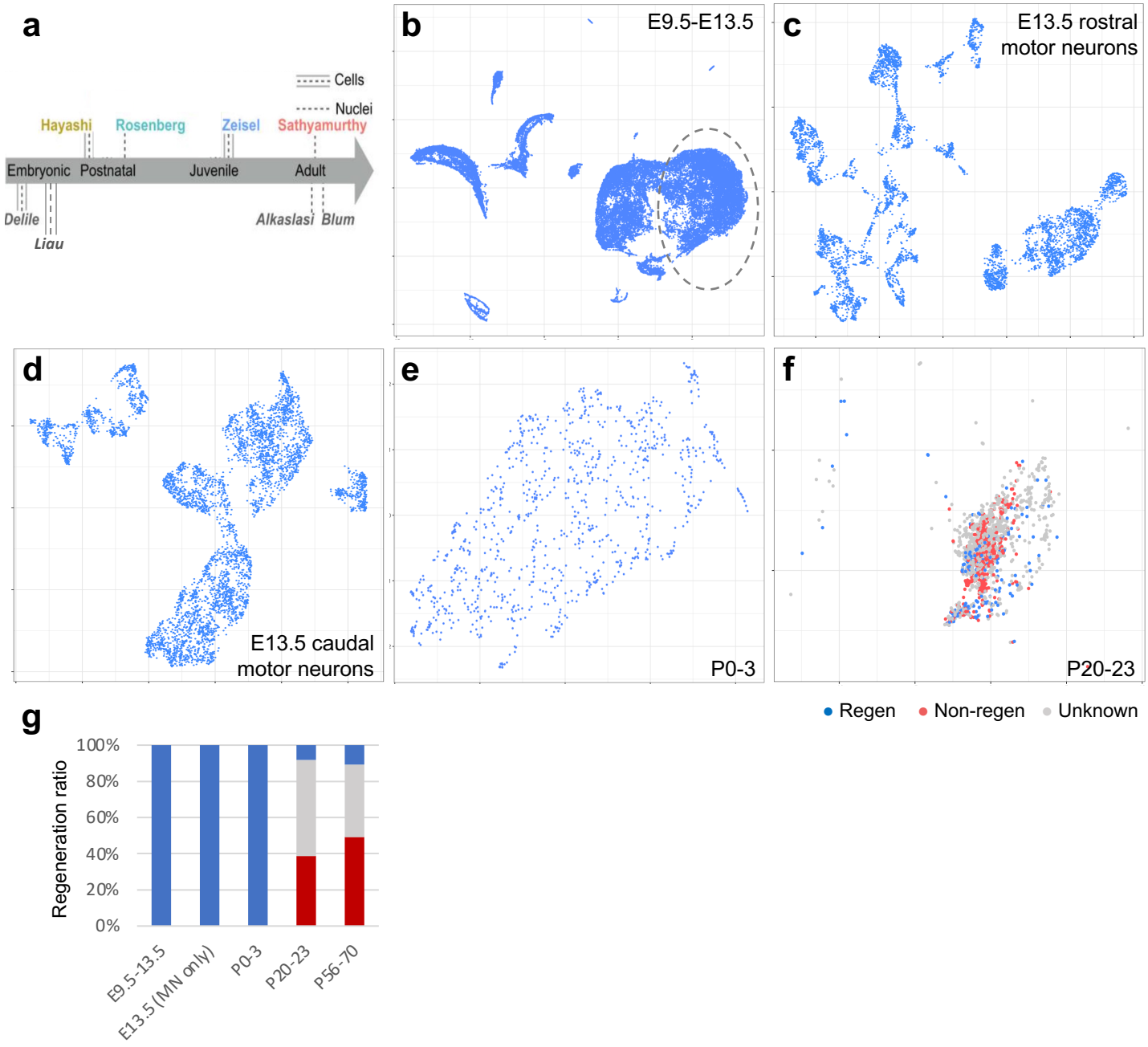


**Extended Data Fig. 6. Applying Regeneration Classifier to spinal cord neurons across developmental stages. a**, A list of datasets analyzed (adapted from Russ et al., 2021). **b-f,** UMAP plots of scRNA-Seq data on spinal cord neurons at different developmental stages, color coded for regeneration classifications. Data are neurons unless marked with a circle that encircles neurons among all cell sequenced. ScRNA-Seq data source: E9.5-13.5, Delile et al., 2019 (all cells); E13.5 spinal motor neurons, Liau et al., 2023; P0-3, Hayashi et al., 2018; P20-23, Zeisel et al., 2018. **g**, Regeneration ratio plot. Data on P56-70 were from Milich et al., 2020 and already presented in Extended Fig. 7 (non-injured control).

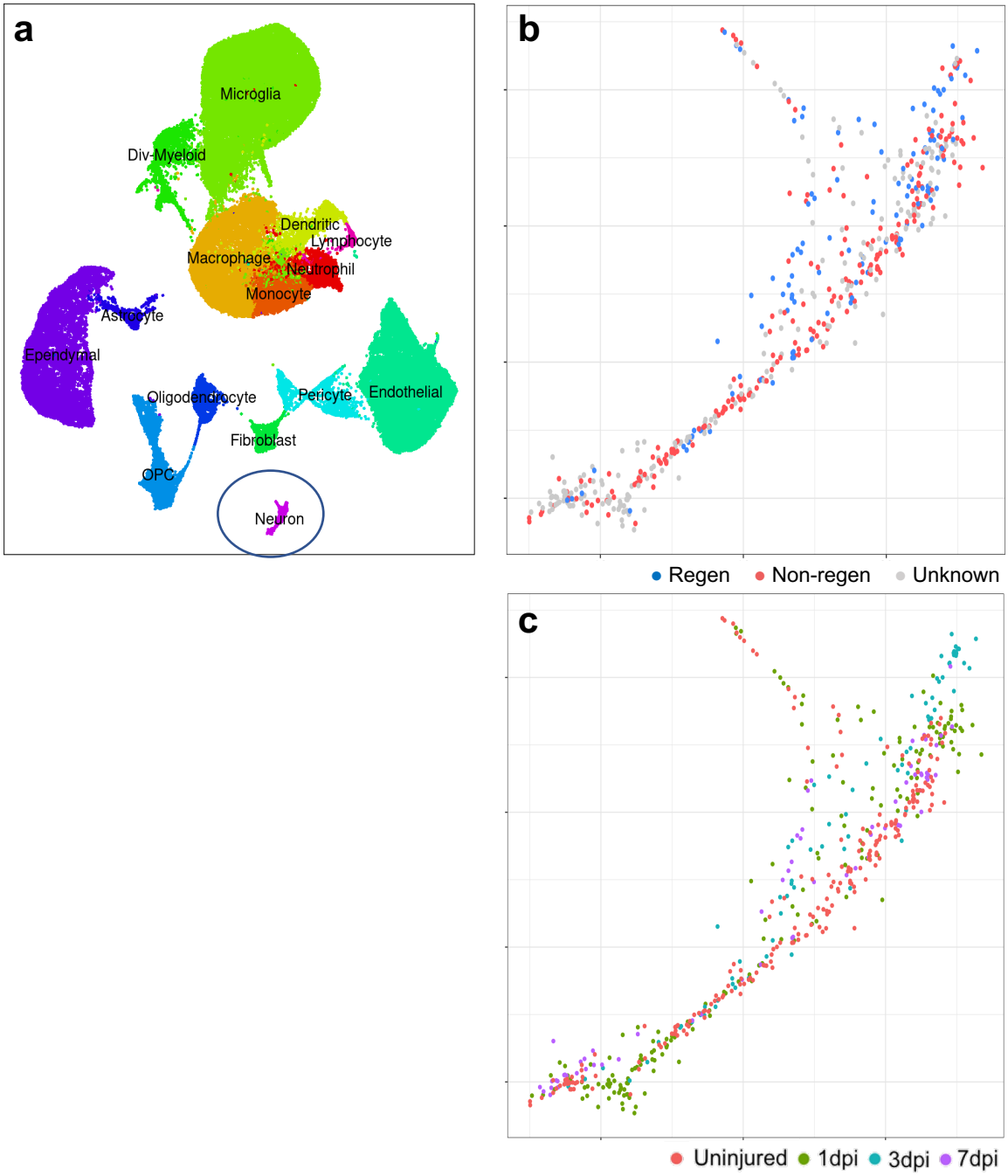


**Extended Data Fig. 7. Applying Regeneration Classifier to cells at a spinal cord injury site from Milich et al., 2021. a**, Original UMAP plot on all cells from Milich et al. 2021. **b**, UMAP plot of neurons only, color coded for regeneration classifications. *The corresponding regeneration ratio plot is shown in Fig. 5a.* **c**, UMAP plot of neurons only color coded for different time points after injury.

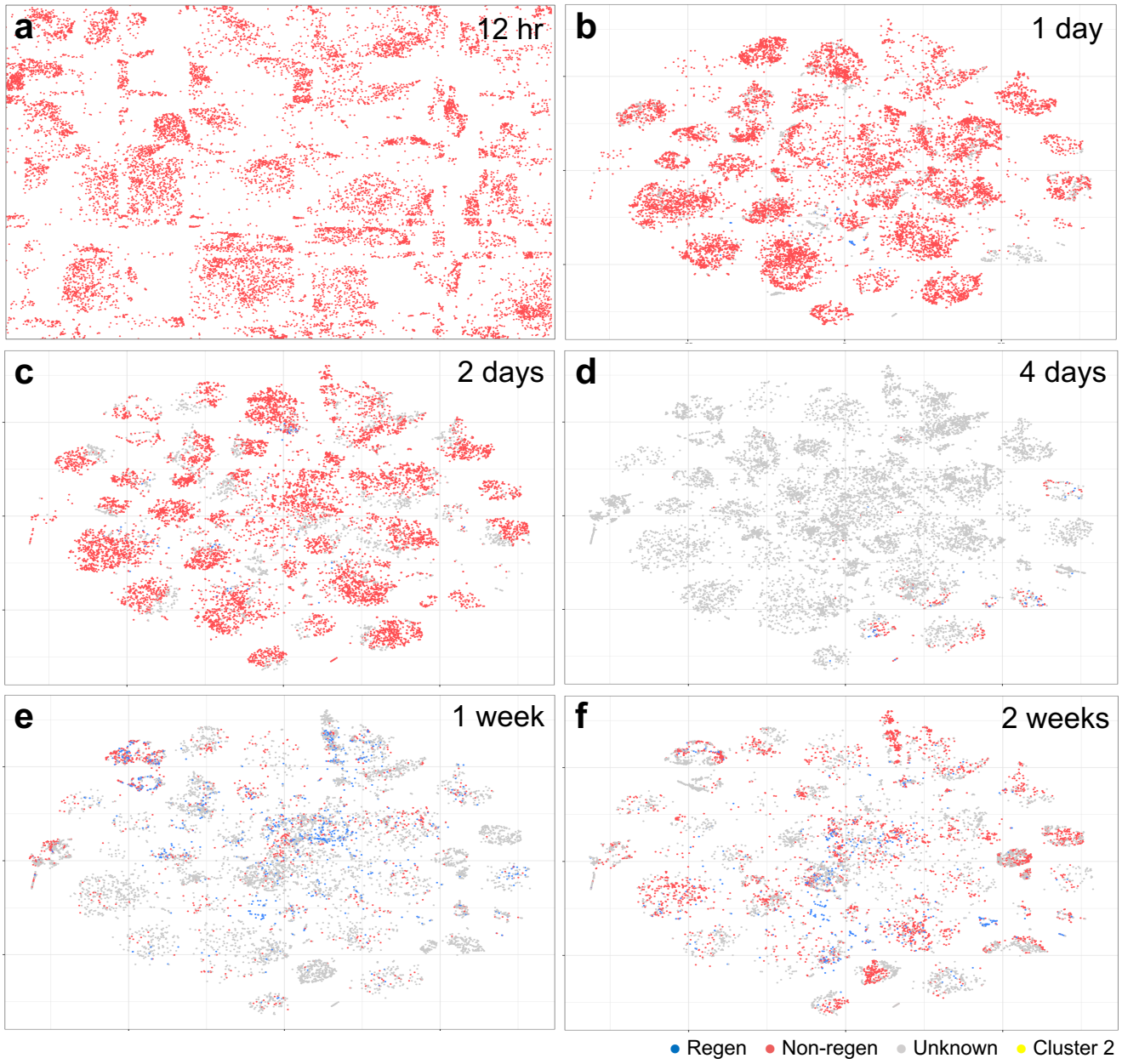


**Extended Data Fig. 8. Applying Regeneration Classifier to retinal ganglion cells (RGCs) after optic nerve crush without molecular interventions from Tran et al., 2019. a-f**, UMAP plots of scRNA-Seq data on adult RGCs at different time points after optic nerve crush, color coded for regeneration classifications. *The corresponding regeneration ratio plot is shown in Fig. 5b.*

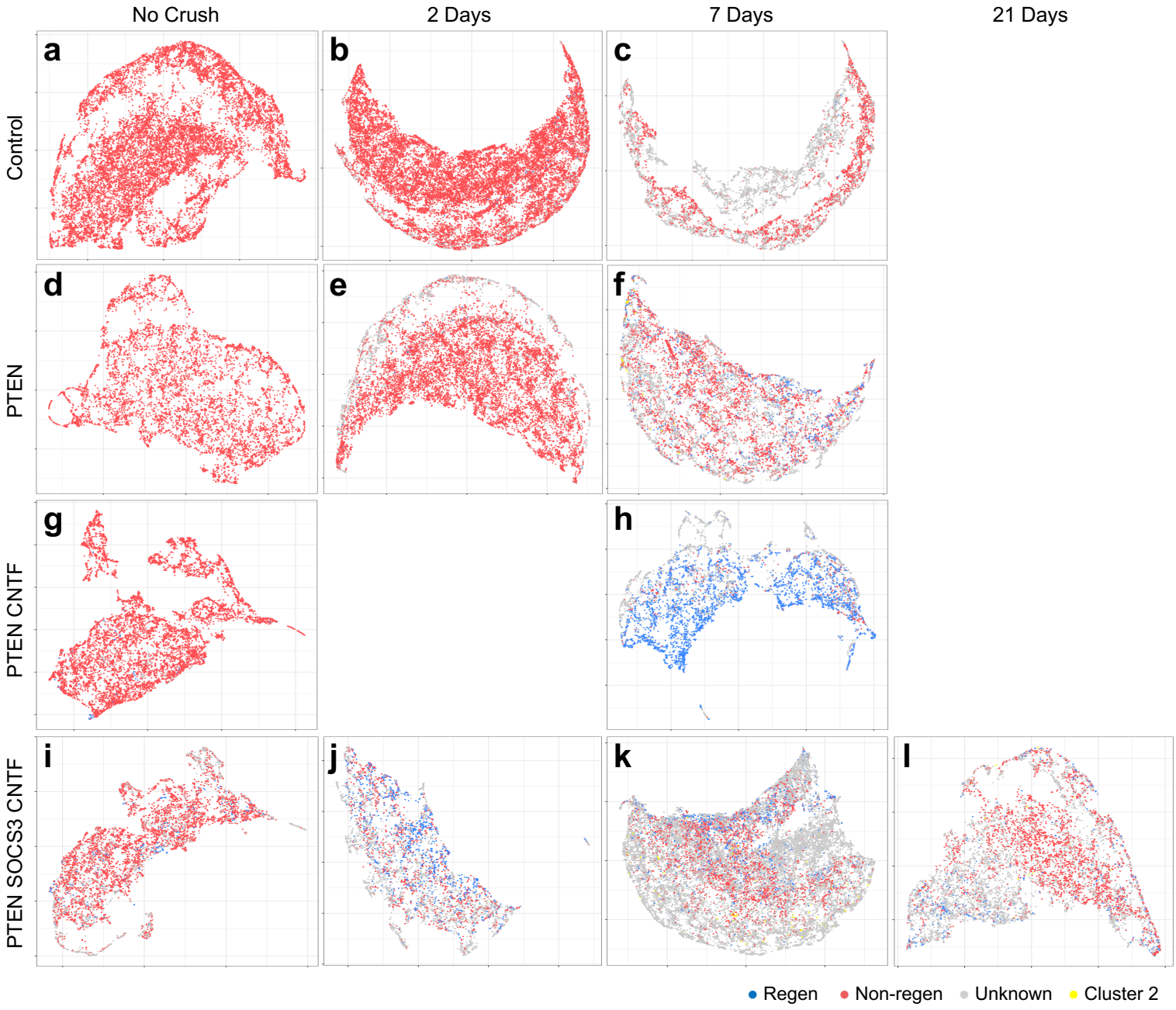


**Extended Data Fig. 9. Applying Regeneration Classifier to retinal ganglion cells (RGCs) after optic nerve crush with molecular interventions by Jacobi et al., 2022. a-l**, UMAP plots or RGCs at different time points after optic nerve crush with various molecular interventions (PTEN/SOCS3 conditional knockout, and/or CNTF overexpression), color coded for regeneration classifications. Blank spaces reflect data points not collected in the original study. *The corresponding regeneration ratio plot is shown in Fig. 5c.*

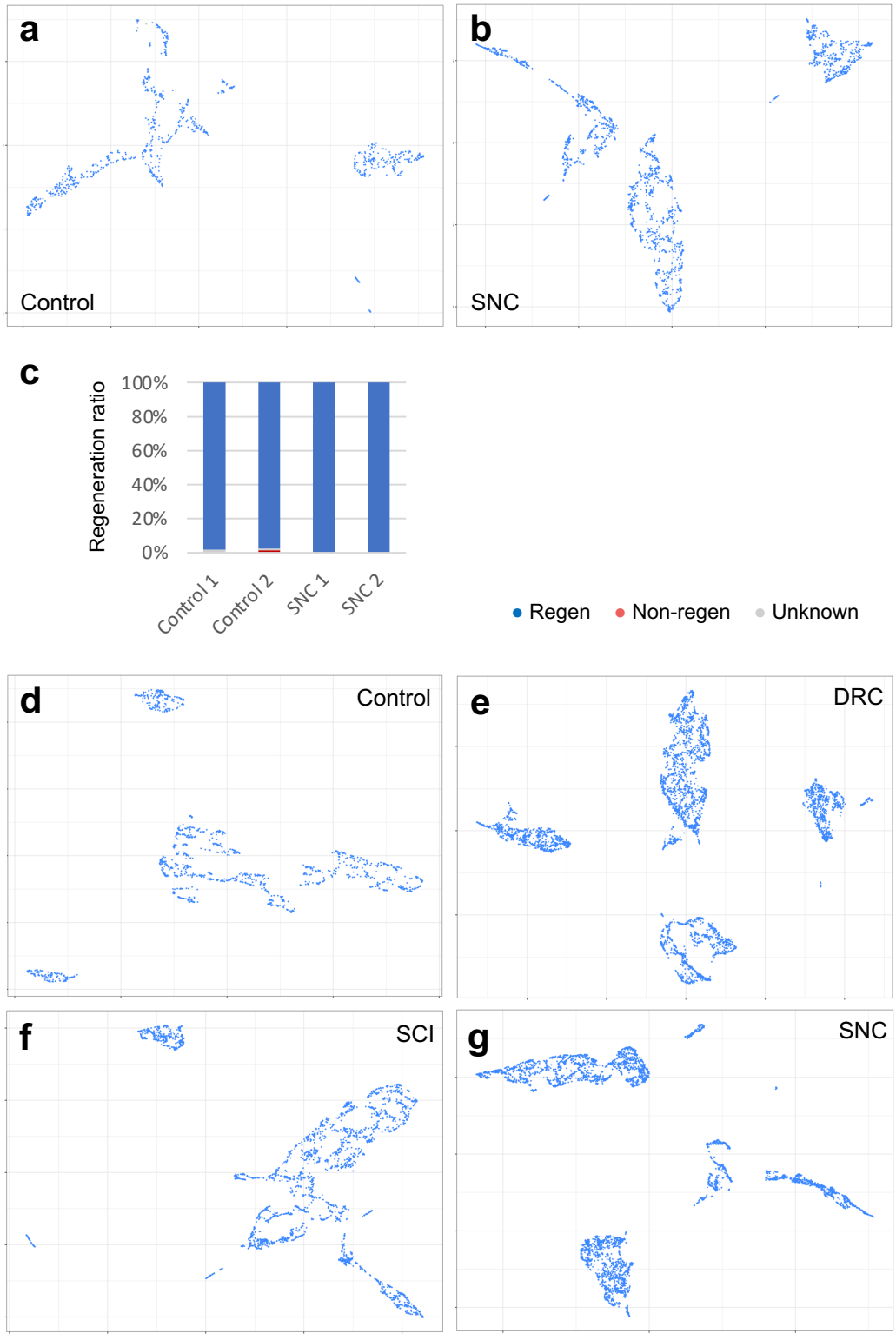


**Extended Data Fig. 10. Apply Regeneration Classifier to adult dorsal root ganglion (DRG) neurons after various injury types. a-b, d-g**, UMAP plot of scRNA-Seq data on DRG neurons after various types of injury, color coded for regeneration classifications. **c**, Regeneration ratio plot for (a, b). *The corresponding regeneration ratio plot for (d-g) is shown in Fig. 5d.* SNC, sciatic nerve crush; DRC, dorsal root crush; SCI, spinal cord injury. ScRNA data source: Avraham et al., 2020 (a-d); Avraham et al. 2021 (d-h).

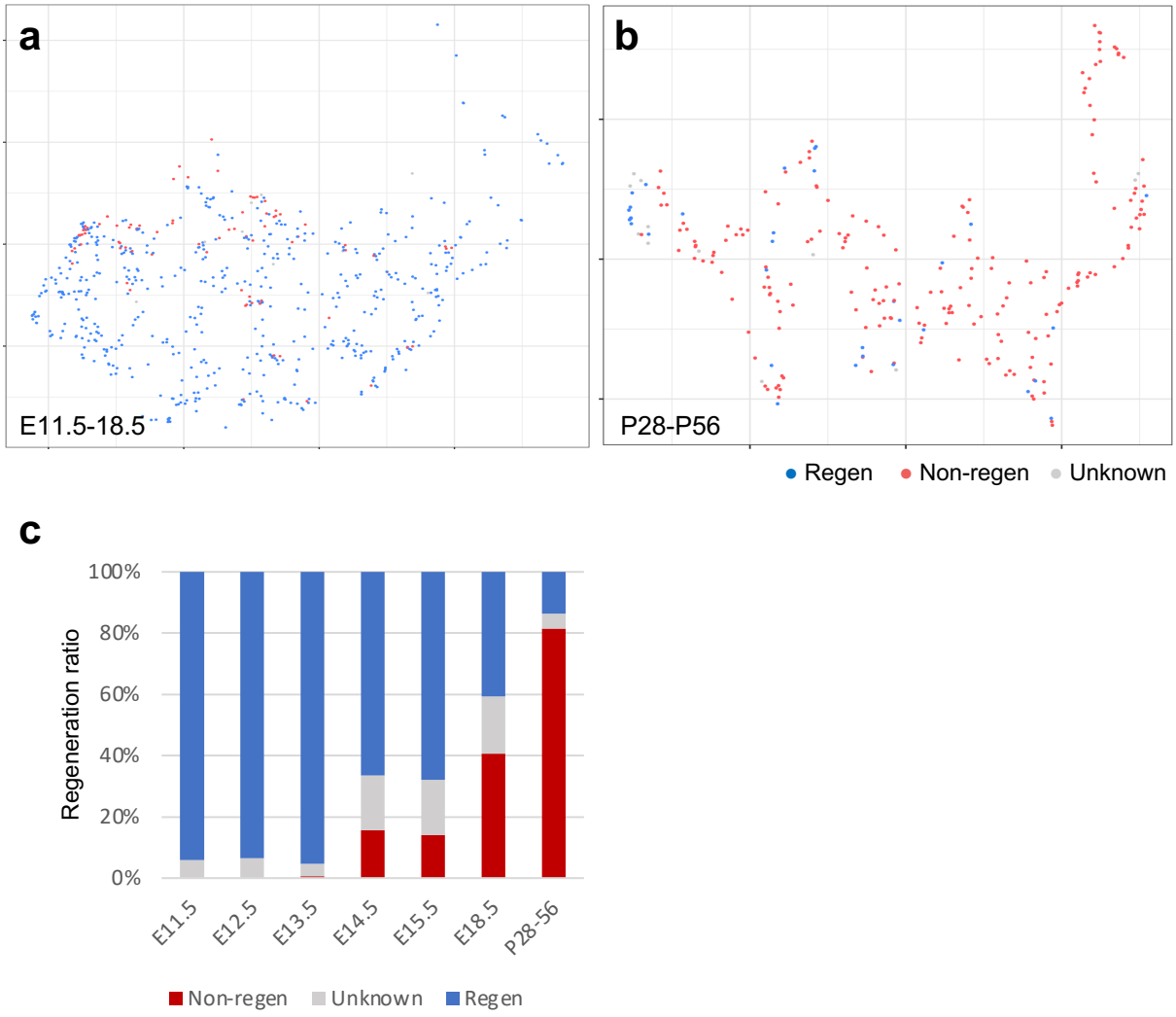


**Supplementary Fig. 1. Applying Regeneration Classifier to embryonic and adult ventral midbrain neurons from LeManno et al., 2016. a**,**b**, UMAP plot of scRNA-Seq data on embryonic (a) and adult (b) neurons only. **c**, Regeneration ratio plot.

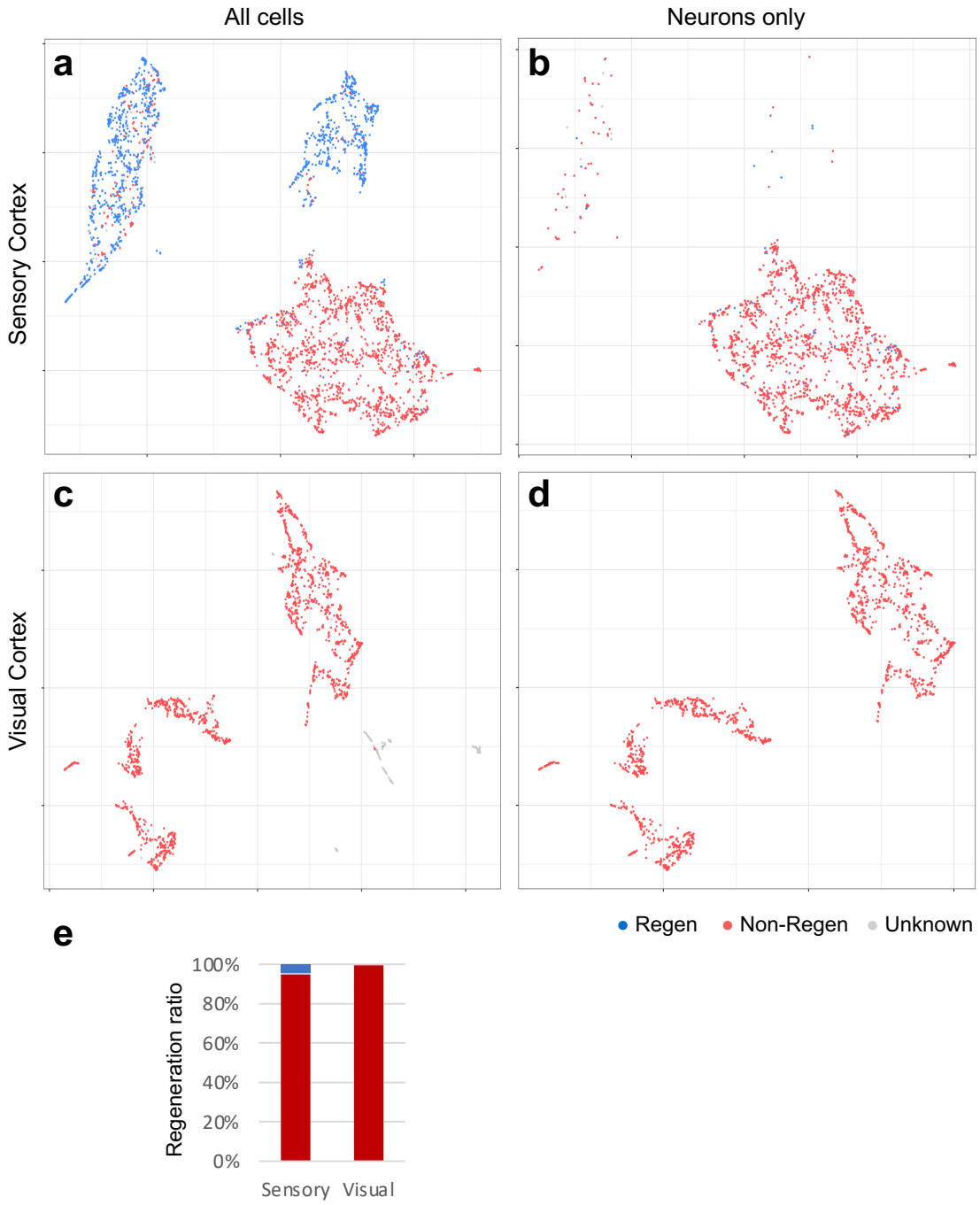


**Supplementary Fig. 2. Apply Regeneration Classifier to adult sensory and visual cortex data. a-d**, UMAP plots of scRNA-Seq data on all cells (a, c) or neurons only (b, d) from sensory (a, b) or visual (c, d) cortex. ScRNA-Seq data source: Zeisel et al., 2015 (sensory cortex), Tasic et al., 2017 (visual cortex). **e**, Regeneration ratio plot on neurons only.

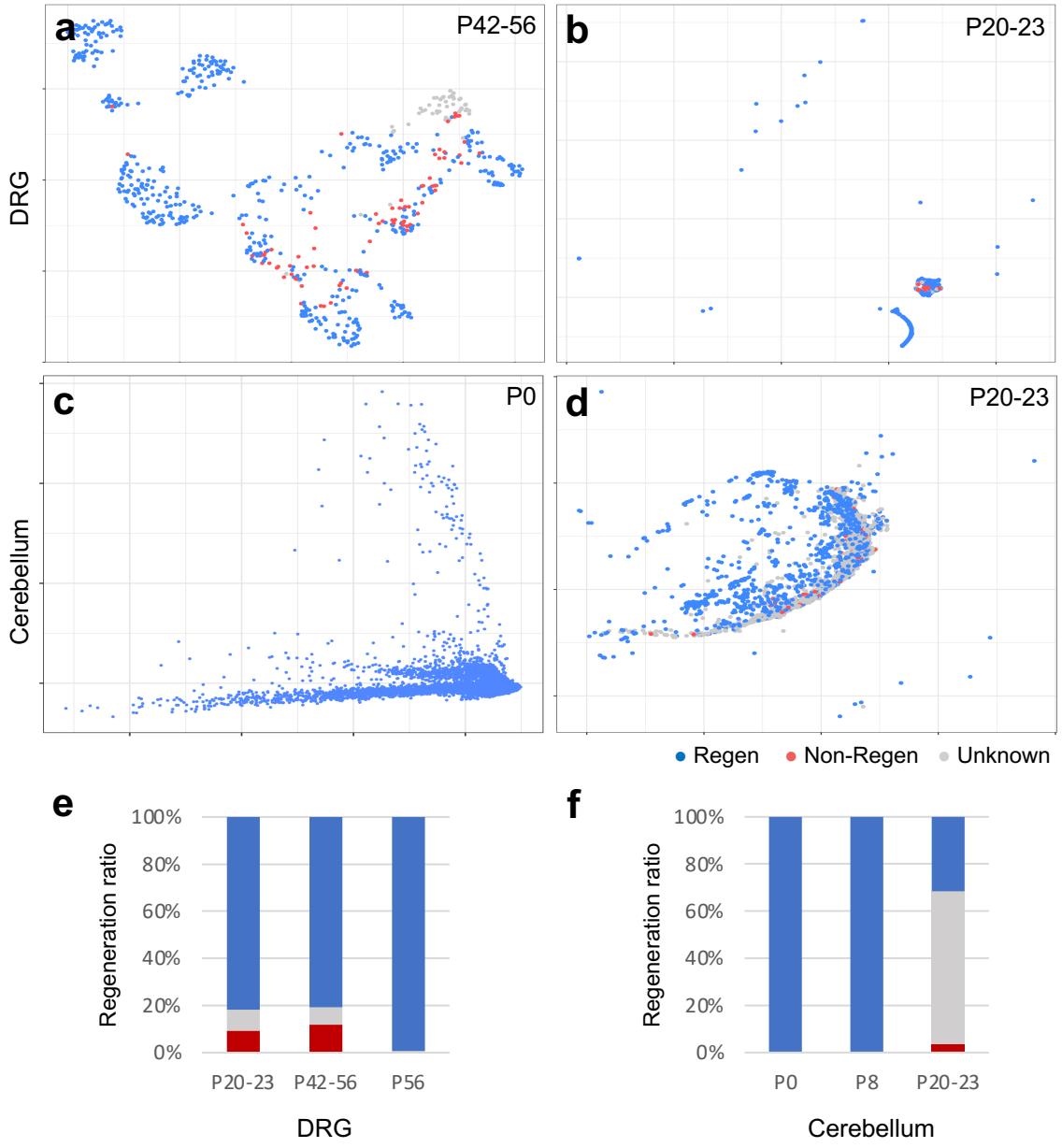


**Supplementary Fig. 3. Applying Regenerating Classifier to dorsal root ganglion (DRG) and cerebellar neurons. a-d**, UMAP plots of scRNA-Seq data on DRG (a, b) and cerebellar (c, d) neurons at different postnatal stages. **e**, Regeneration ratio plot of DRG neurons (UMAP of P56 is shown in Extended Data Fig. 10). Note that data on DRGs from P20-23 and P42-56 were done with older technologies. **f**, Regeneration ratio plot of cerebellar neurons. ScRNA-Seq data source: P42-56, Usoskin et al., 2015; P20-23 (both DRGs and cerebellum), Zeisel et al., 2018; P0-8, Peng et al., 2019.

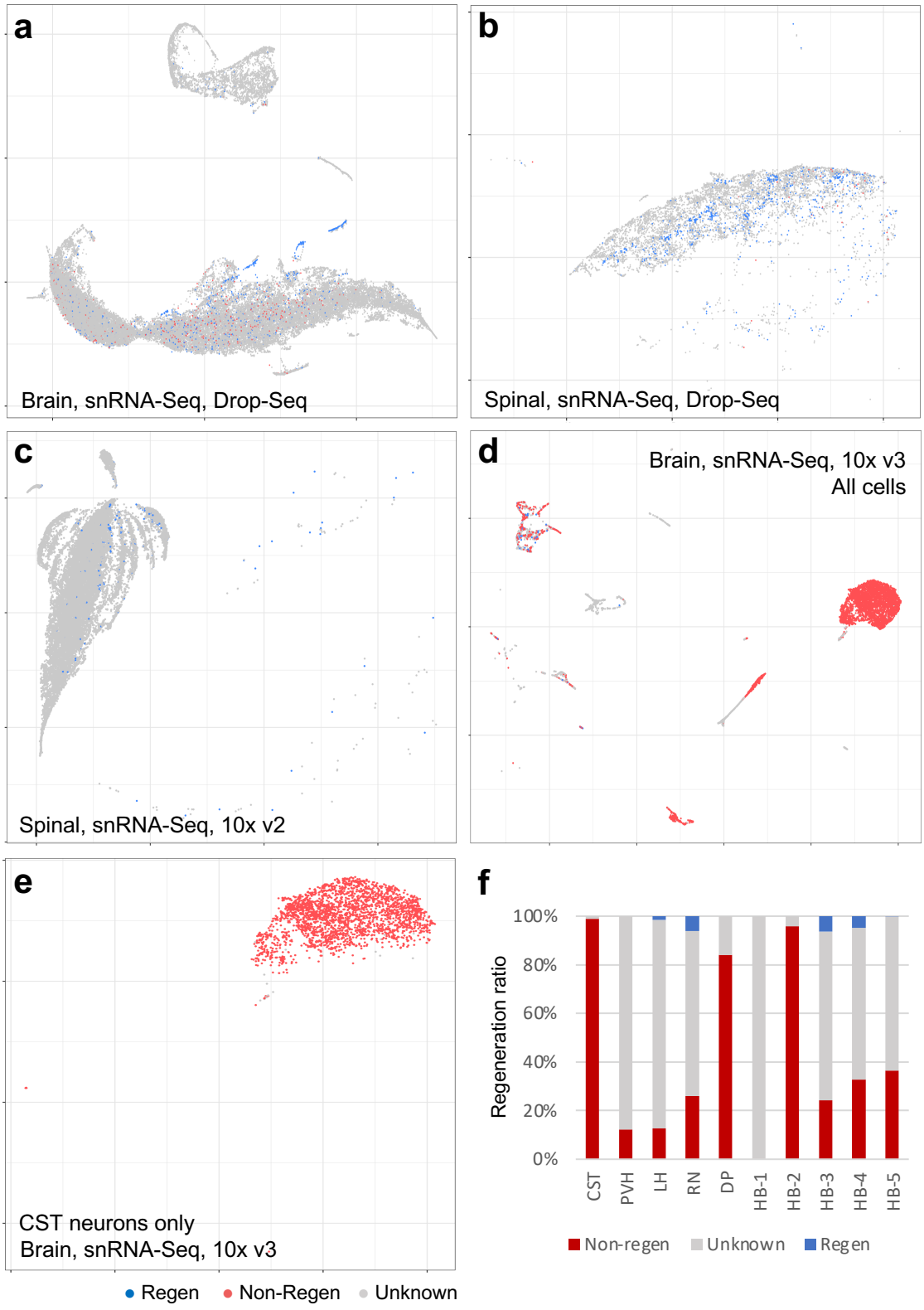


**Supplementary Fig. 4. Applying Regeneration Classifier to snRNA-Seq data was less informative. a-c**, UMAP plots of snRNA-Seq on all cells from Hu et al., 2017 (a); spina cord cells from Sathyamurthy et al., 2018 (b); spinal cord neurons from Matson et al., 2022. **d**,**e**, UMAP plots of scRNA-Seq data on all cells (d) or CST neurons only (e) from Beine et al., 2022. **f**, Regeneration ratio plot on neurons from different brain regions in Beine et al., 2022. CST, corticospinal tract; PVH, paraventricular hypothalamus; LH, lateral hypothalamus; RN, red nucleus; DP, dorsal pons; HB, hindbrain (HB1-5 are five different single nucleus clusters in Beine et al., 2022). Note that out of four snRNA-Seq studies, only the study using 10x v3 generated informative results, likely reflecting a higher complexity per nucleus for v3.